6588 *Macromolecules* **2010**, *43*, 6588–6598
DOI: 10.1021/ma100726z

Macromolecules
ARTICLE

# Langmuir−Schaefer (LS) Macroinitiator Film Control on the Grafting of a Thermosensitive Polymer Brush via Surface Initiated-ATRP

**Nicel C. Estillore, Jin Young Park, and Rigoberto C. Advincula***

*Department of Chemistry and Department of Chemical Engineering, University of Houston, Houston, Texas 77204-5003*

*Received April 5, 2010; Revised Manuscript Received July 4, 2010*

ABSTRACT: A novel surface modification based on the Langmuir−Schaefer (LS) monolayer technique was utilized for controlled surface-initiated atom transfer radical polymerization (SI-ATRP) of polymer brushes. The fabrication of these films was prepared by spreading an insoluble monolayer of an amphiphilic macroinitiator, poly(styrene-*copolymer*-hydroxyethyl methacrylate-2-bromoisobutyryl bromide) (p(St-*co*-HeBiB)), capable of initiating the ATRP polymerization of *n*-isopropylacrylamide (NIPAM). During the LS monolayer deposition, the surface pressure was varied in order to probe its effect on the initiator distribution and subsequent grafting density and thickness. The surface-bound macroinitiator ranged from a loosely (low surface pressure) to a densely (high surface pressure) crowded initiation sites on a monolayer. Increasing LS macroinitiator film thicknesses were observed with deposition at increasing surface pressures, i.e. 5, 15, 20, 30, and 50 mN/m using ellipsometry. However, based on the XPS data, there was a decrease in the bromine signal for the 50 mN/m LS macroinitiator film. Contrary to this result, there was a higher nitrogen signal and thicker pNIPAM brushes obtained for the 50 mN/m LS brush film. This was explained by a macroinitiator surface rearrangement during polymerization accounting for the difference. Moreover, wetting measurements by static water contact angle and an *in situ* atomic force microscopy (AFM) experiment were performed to investigate the temperature dependence of the pNIPAM brush surface wettability and morphology, respectively.

## Introduction

The fabrication of ultrathin films that respond to external stimuli such as pH, solvent, temperature, and light are of fundamental interest especially for applications such as ion selectivity,[1−3] controlled release,[3−5] polymer coatings,[6,7] and optical devices.[8] High density surface tethered polymer chains are particularly attractive for these types of smart surfaces and coatings because they can undergo conformational (i.e., swelling and collapsing) changes as a result of an external stimulus. At the same time, by anchoring at one end, it is possible to observe reversibility of the tethered polymer chains. Grafted poly(*n*-isopropylacrylamide) (pNIPAM) is among the most studied stimuli-responsive films due to the polymer's ability to respond to a lower critical solution temperature (LCST) of 32 °C.[5,7,9−12] phase transitions from coil to globule and globule to coil are observed above and below the LCST which are attributed to the alterations in the hydrogen-bonding interactions of the amide group.[12] Because of this phenomenon, thermoresponsive surfaces have been applied to drug delivery,[13] ion gating,[4,14] nanopatterning applications,[15−17] and chromatographic separation media for organic and biological molecules.[18]

While the physisorption method has been employed for synthesizing tethered polymer chains to an interface,[19] the chemisorption method is now considered the most commonly and widely used method for grafting as it overcomes the limitations inherent with physisorbed films, namely weaker adhesion of the polymer chains to the surface.[20] The most notable methods are the "grafting to" and "grafting from" techniques which covalently graft polymer chains to an interface.[20] Surface initiated polymerization (SIP) or "grafting from" is commonly preferred over the "grafting to" method for preparing surface bound polymer chains having various morphologies as mushroom, pancake, and brush.[20] The "grafting to" method is based on the reaction between the anchor group of a preformed polymer with the reactive functionalities on the surface. This method is intrinsically limited to low surface grafting density and low film thickness as the grafted polymer chains inhibit the diffusion of the incoming chains to the available reactive sites on the surface due to overcrowding. On the other hand, the "grafting from" method is based on the *in situ* polymerization of monomers from the surface (i.e., polymer growth is initiated from the surface).[20] Grafted polymer brushes are grown from surface bound initiators with a sufficiently high grafting density such that the polymer chains are forced to stretch away or in the direction perpendicular to the surface. Traditional free radical polymerization which uses a derivatized 2, 2′-azobis(isobutyronitrile) (AIBN) initiator has been widely used for the preparation of polymer brushes.[21] However, recent advances in controlled living radical polymerizations (CLRP) such as atom transfer radical polymerization (ATRP),[22,23] reversible addition−fragmentation chain transfer (RAFT) polymerization,[24] and nitroxide-mediated polymerization (NMP)[25] have led to more complex brush architectures. ATRP is arguably the most widely used CLRP technique for the synthesis of well-defined polymer brushes with controlled molecular weights and narrow polydispersity indices (PDI).[22] Furthermore, ATRP allows for the formation of block copolymers by simply reinitiating the dormant chain ends and subsequently extending the polymer chains.

SIP generally starts out with the immobilization of surface bound initiators. Besides the conventional casting methods (i.e., spin and dip coating), various other techniques such as formation of self-assembled monolayer (SAM),[21,26] vapor deposition,[27] electrostatic self-assembly using polyelectrolyte macroinitiators,[28]

*radvincula@uh.edu.

 Published on Web 07/21/2010 

layer-by-layer (LbL) method,[3,29−31] and most notably the Langmuir−Blodgett (LB) technique[32−35] have all been successfully applied. Unlike the former surface modification techniques which rely on the random adsorption of initiator molecules onto the substrate surface, the latter technique in principle should allow precise control over the packing density of initiator molecules. The LB technique has been used extensively for making very stable monolayers at the air−water interface and even multilayer when transferred to a solid support.[36] Block or triblock copolymers are particularly interesting for LB studies since they have the ability to phase separate at the air−water interface with the polar head group preferentially at the water subphase while the nonpolar tail group at the air interface. Furthermore, amphiphilic polymer monolayers spread at the air−water interface are of fundamental interest in understanding the polymer−polymer and polymer−interface interactions.[37] Depending on the nature of the substrates used during the monolayer transfer onto a solid support, either the LB vertical method or the Langmuir−Schaefer (LS) horizontal method can be used.

In addition to immobilizing the initiator onto a substrate surface, control of the initiator density must also be taken into consideration. Precise control of the surface bound initiators requires the ability to account for the number of available active initiating sites on the surface. The most common technique employed is to control the concentration of the initiator solution during the self-assembly of the monolayer as well as the length of time the substrate surface is in contact with the initiator solution. Another is the mixed monolayer approach where an active species (i.e., ATRP initiator) and an inert analogue are used.[38,39] Genzer et al. applied the gradient approach using the vapor deposition method which led to studies on the mushroom-to-brush transition as well as the wettabilities of the different regions on the surface.[27] Luzinov et al. also employed a similar approach to create temperature gradient surfaces.[40] Photodecomposition of active sites as a means to control initiator density has also been reported.[41,42] In a recent publication, our group demonstrated the use of the LbL technique and SI-ATRP for the fabrication of pH and temperature sensitive films.[3] It was concluded that by successively depositing alternating layers of the polyelectrolyte macroinitiators, this translated to more initiating sites available for the polymerization resulting in thick pNIPAM brushes. Armes and co-workers have also demonstrated the sole deposition of polyelectrolyte macroinitiators by the LbL technique on planar substrates and the subsequent graft polymerization of pHEMA brushes.[29]

Fukuda et al. were the first to report the controlled graft polymerization of various monomers by combining the LB and SI-ATRP techniques.[32−35] In these studies, a small molecule was used as the ATRP initiator for the polymerization of methyl methacrylate (MMA)[32] and a sugar carrying monomer (MAIpG1c).[33] The spreading of the initiator solution at the air−water interface was followed by a hydrolysis reaction on the water surface. The covalent attachment of the initiator onto a silicon wafer substrate was done by vertically transferring the initiator monolayer at a constant surface pressure. However, these studies only focused on the controlled graft polymerization of monomers using the surface pressure at which the most stable monolayer was formed. The effect of varying the surface pressure on initiator packing density was not investigated. Therefore, we propose that the initiator packing density can be controlled by varying the applied surface pressure which will then play a key role in dictating the polymer brush growth and morphology of the surface tethered polymer chains.

In this paper, we report the surface immobilization of an amphiphilic macroinitiator based on the LS technique and SI-ATRP polymerization of a temperature sensitive polymer brush, pNIPAM. In particular, we synthesized a 3:1 ratio of styrene to a bromoester ATRP initiator via free radical polymerization yielding a statistical copolymer of p(St-*co*-HeBiB) amphiphilic macroinitiator. A relatively high initiator density on the surface is necessary for the tethered polymer chains to attain the brush morphology. Therefore, various surface pressures were used during the transfer of the monolayer onto a solid surface in order to shed light of their effect on the initiator packing density. In addition, the effects of polymerization time and monomer concentration on the growth of the brushes were also investigated. Finally, a wetting experiment by static water contact angle and an *in situ* AFM experiment were performed to investigate the temperature dependence of the pNIPAM brush surface wettability and morphology, respectively.

## Experimental Section

**Materials.** 2-Hydroxyethyl methacrylate (HEMA; 98% Aldrich) and styrene (St; Reagent Plus, 99% Aldrich) were passed through an activated basic alumina column to remove the inhibitor. *N*-Isopropylacrylamide (NIPAM; >98% TCI America) was recrystallized from hexane. 2-Bromoisobutyryl bromide (2-BiBB; 97% TCI America), *N*,*N*,*N*′,*N*′,*N*″-pentamethyldiethylenetriamine (PMDETA; 99% Aldrich), 2,2′-azobis(isobutyronitrile) (AIBN; 98% Aldrich), and $Cu^{I}Br$ (98% Alfa Aesar) were used as received without further purification. HPLC chloroform (J. T. Baker) solvent was used for the LS experiments. Milli-Q water with resistivity of 18 MΩ was used for the LS experiments and polymerizations. Tetrahydrofuran (THF) was freshly distilled and collected immediately prior to use.

**Instrumentation.** $^{1}$H NMR spectra were recorded on a General Electric QE 300 spectrometer (300 MHz). Fourier transform infrared (FT-IR) absorption spectra of pNIPAM brush films on silicon substrates were measured with a Digilab FTS7000 series spectrometer (Varian). Spectra (4000−700 $cm^{-1}$) were collected at 4 $cm^{-1}$ resolution using a mercury−cadmium−telluride (MCT) detector with 512 scans being averaged per spectrum. KBr pellets were prepared from amphiphilic macroinitiator dried in a vacuum oven for 24 h at room temperature (RT).

Thermogravimetric analysis (TGA) measurements were made on a TA Instruments model 2920 using $N_2$ purge gas and a platinum pan. The samples were heated up to 1000 °C at a heating rate of 20 °C/min using the ramp method. Differential scanning calorimetry (DSC) measurements were made on a TA Instruments model 2950 using $N_2$ purge gas and an aluminum pan. The heat/cool/heat method was employed with an onset temperature of 21 °C. $T_g$ was determined by DSC from the midpoint of the inflection tangent from the second heating at 5 °C/min. The Curie temperature standard method along with a ferromagnetic material (Nickel) and a low melting indium sample were used to perform temperature and enthalpy calibrations on the TGA and DSC instruments, respectively. TGA and DSC data were analyzed using TA Instruments Universal Analysis Software. Static water contact angle goniometry was conducted using a KSV CAM 200 instrument (KSV ltd.).

Gel permeation chromatography (GPC) analysis was performed at room temperature using a Viscotek 270 (Viscotek, Inc.) equipped with a VE3580 RI detector and a three column series including two GMHHR-M (maximum pore size 500 nm) and one GMHHR-L (maximum pore size 150 nm) Mixed Bed ViscoGel column. THF (Omnisolve, HPLC grade) was used as the eluting solvent with a flow rate of 1 mL $min^{-1}$. Samples were prepared at a concentration of 1 mg $mL^{-1}$ and an injection volume of 100 μL was used. Monodisperse poly(styrene) and polydisperse poly(methyl methacrylate) standards (EZ Vials, Polymer Laboratories) were used to construct the calibration curves.

A Langmuir−Blodgett trough (KSV 2000 Ltd.) with two symmetric barriers was used for all the surface pressure vs mean molecular area isotherms as well as for the dipping experiments.

Langmuir−Schaefer (LS) horizontal technique was used for the transfer of the monolayer onto a hydrophobic silicon wafer substrate.

X-ray photoelectron spectroscopy (XPS) was carried out on a Physical Electronics 5700 instrument with photoelectrons generated by the nonmonochromatic Al KR irradiation (1486.6 eV). Photoelectrons were collected at a takeoff angle of 45° using a hemispherical analyzer operated in the fixed retard ratio mode with an energy resolution setting of 11.75 eV.

Null ellipsometry was used to determine the thicknesses of the LS macroinitiator and pNIPAM brush films. All measurements were conducted using a null-ellipsometer operating in polarizer-compensator-sample-analyzer (Multiskop, Optrel Berlin) mode. As a light source, a He−Ne laser ($\lambda = 632.8$ nm) was applied, and the angle of incidence was set to 60°. A multilayer flat film model was used to calculate the LS macroinitiator and pNIPAM brush thicknesses from the experimentally measured ellipsometric angles $\Delta$ and $\Psi$, assuming refractive indices of 1.43 for the LS macroinitiator films and 1.50 for the pNIPAM brush films.

All atomic force microscopy (AFM) images were recorded in air under ambient conditions on a PicoScan system (Agilent Technologies formerly Molecular Imaging Corp.) equipped with an $8 \times 8$ $\mu$m scanner. Magnetic AC (MAC) mode (noncontact mode) was used for all imaging. A MAC lever, which is a silicon nitride-based cantilever coated with magnetic film, was used as an AFM tip. The temperature dependent study on the pNIPAM brush films was conducted using an automatic temperature controller.

**Free Radical Polymerization of Amphiphilic Macroinitiator, p(St-*co*-HeBiB).** The free radical copolymerization of the amphiphilic macroinitiator was conducted using a 3:1 ratio of the styrene (St) monomer to HeBiB (2-hydroxylethyl methacrylate-2-bromoisobutyryl bromide) monomer. In a Schlenk flask equipped with a small stir bar, 2.0 mL of styrene (17.40 mmol), 1.619 g of HeBiB (5.799 mmol), and 95.23 mg of AIBN (0.580 mmol) were dissolved in 10 mL of dry THF. To remove any dissolved gases and impurities, the reaction mixture was put under six freeze−pump−thaw cycles. The flask was placed into a thermostated oil bath set at 60 °C for 6 h. The polymerization was terminated by repeated exposure to air. The polymer was precipitated from excess hexane and dried under vacuum prior to use. (65.9% product yield and $^1$H NMR spectrum is provided in the Supporting Information. GPC analysis: $M_n = 10\,938$, $M_w = 15\,314$, and PDI = 1.40).

**Monolayer Deposition.** The amphiphilic macroinitiator, p(St-*co*-HeBiB), was spread from a chloroform solution (1 mg/mL) on a clean water surface in a standard LB trough having a subphase volume of 240−700 mL. The surface pressure was measured by a Wilhelmy-type film balance. A 50 $\mu$L of the macroinitiator solution was injected using a microsyringe at different locations on the water subphase. After spreading the solution, the solvent was evaporated for 15 min. The monolayer was compressed at a constant surface pressure at a rate of 10 mm/min. The monolayer deposition was done using the LS technique on a silicon wafer substrate (pretreated with hydrofluoric acid) at a rate of 1 mm/min.

**ATRP Polymerization of NIPAM.** The polymerization of NIPAM was conducted at ambient conditions in an aqueous media in the presence of $Cu^IBr$/PMDETA catalyst system. The optimization of the polymerization condition has been done in our previous publication.[3] Briefly, in a 50 mL Schlenk flask equipped with a small stir bar, a solution of NIPAM (2.0 g, 17.674 mmol), PMDETA (111 $\mu$L, 0.530 mmol) and $Cu^IBr$ (25.4 mg, 0.177 mmol) in a mixed solvent of $H_2O$/MeOH (2.0 mL/2.0 mL, 1:1 v:v) was degassed for 1 h to remove any dissolved gases and impurities. A homogeneous (green) solution of the monomer and transition metal/ligand complex was transferred using a cannula to a different Schlenk flask containing an LS macroinitiator film. The polymerization was conducted at RT for 2 h under a $N_2$ atmosphere. The polymerization was terminated by exposing the reaction flask to air and rinsing the substrates repeatedly with copious water and methanol to remove residual catalyst. The substrates were then subsequently dried under vacuum prior to surface analysis. A similar procedure was conducted for [NIPAM] = 0.5 and 2.0 M with polymerization times 1, 2, 4, and 8 h. The polymer brush films were characterized by ellipsometry, static water contact angle goniometry, FT-IR, XPS, and AFM (refer to the Results and Discussion).

## Results and Discussion

**Amphiphilic Macroinitiator Synthesis, p(St-*co*-HeBiB).** The amphiphilic macroinitiator with a molar ratio of 3:1 styrene to HeBiB was synthesized via free radical polymerization (Scheme 1a). The resulting statistical copolymer, p(St-*co*-HeBiB), forms an insoluble amphiphilic monolayer when a solution of it is spread at an air−water interface with the pSt segment at the air interface while the pHeBiB segment (ATRP initiator) at the water subphase. An ATRP bromoester based initiator was chosen due to its higher initiation efficiency as compared to an amide based initiator.[22] In addition, the abstraction of the bromine atom should be relatively facile since a 3° radical is formed. GPC traces of the copolymer provided a molecular weight of 15 314 g/mol along with a relatively broad PDI value of 1.40. FT-IR analysis confirms the successful copolymerization of the macroinitiator (Supporting Information Figure S2). Since a 3:1 ratio was used for styrene to HeBiB, an intense aromatic −CH stretching and −C═C bending at 3030 and 1650 cm$^{-1}$ were observed, respectively. The −CH, $-CH_2$, and $-CH_3$ stretches of the polymer backbone were observed between 2900 and 3000 cm$^{-1}$. There was also an intense carbonyl ester stretch (−C═O) at 1750 cm$^{-1}$ due to the pHeBiB segment of the copolymer.

TGA and DSC analyses were performed to investigate the thermal properties of the copolymer. The macroinitiator shows a good thermal stability when heated up to 200 °C where an initial 8−10% weight loss is observed due to water and moisture. The first major weight loss, however, occurred at about 330 °C due to the decomposition of the weakly bonded bromoester segment of pHeBiB.[43] The second major thermal decomposition at 400 °C is due to the pSt segment of the copolymer.[43] The copolymer also displayed a relatively low glass transition temperature, $T_g$, of 38.5 °C. This value is low compared to a copolymer consisting of polystyrene-poly(methyl methacrylate)[44] and is attributed to the incorporation of the bromoester segment of pHeBiB.

***$\pi$−A* Isotherm of p(St-*co*-HeBiB).** The immobilization process of the p(St-*co*-HeBiB) macroinitiator which was spread from a chloroform solution and allowed to evaporate for 15 min is shown in Scheme 1b. Figure 1 shows the surface pressure ($\pi$) vs mean molecular area ($A^2$) per polymer molecule occupied by the macroinitiator at a subphase temperature of 21 °C and constant barrier speed of 10 mm/min. As the surface pressure increased, the occupied area by the macroinitiator decreased and the estimated limiting area by extrapolating the steepest tangent of the isotherm to zero surface pressure was about 10 nm$^2$. A lower limiting area value of 0.35 nm$^2$ was reported by Fukuda et al. and is mainly due to the difference in the sizes of the initiating species used.[32] Furthermore, the macroinitiator used in this study has a molecular weight of 15 314 g/mol and a broad PDI value of 1.40; thus it will occupy a bigger area as compared to a smaller molecule which can be compressed to a very small area. It can also be seen in the isotherm that a condensed type monolayer is formed which is evident by a sharp increase in $\pi$ as A decreases. The macroinitiator used in this study has a similar behavior to a polystyrene−poly(methyl methacrylate)

**Scheme 1. (a) Amphiphilic Macroinitiator Synthesis via Free Radical Polymerization, (b) Monolayer Deposition by the Langmuir−Schaefer (LS) Horizontal Technique and (c) ATRP Polymerization of NIPAM**

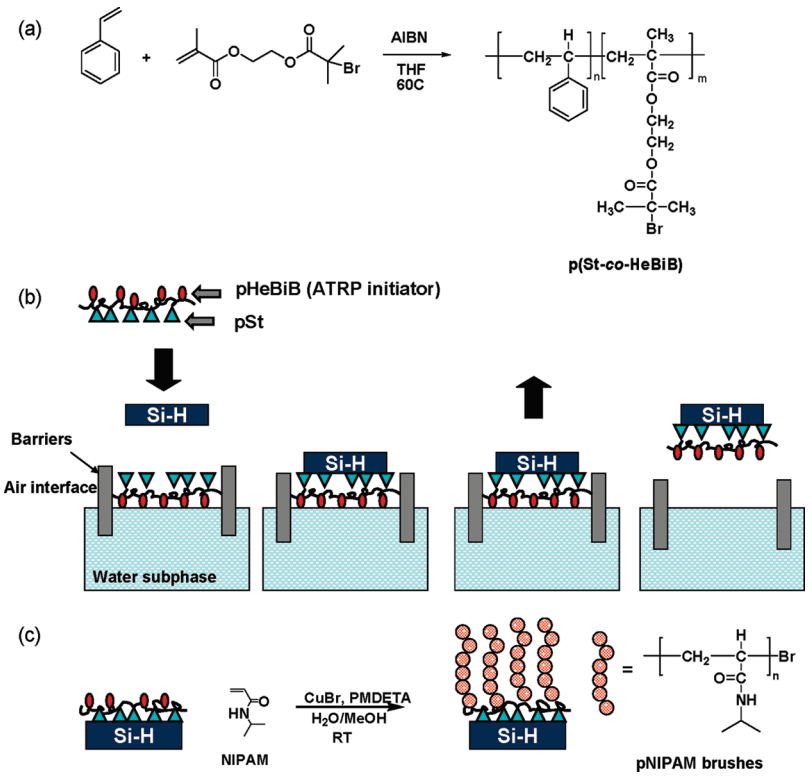


(PSt−PMMA) diblock copolymer. The Langmuir monolayers of PSt and PMMA homopolymers and PSt−PMMA diblock copolymer have been extensively studied.[37,45−50] Kumaki as well as other groups reported very small limiting areas for polystyrene indicating that it forms as flakes or multilayer when spread on the water subphase.[46b,47,48] PMMA forms a condensed type monolayer as evident by its rather small limiting area compared to an expanded type monolayer (i.e., poly(ethylene oxide) and poly(vinyl acetate)) as well as in its sharp increases in $\pi$ as A decreases.[49] Polymers with sufficiently hydrophilic groups in the repeating unit such as poly(vinyl acetate) are known to spread ideally on the water subphase forming very stable monolayers.[49] However, in the case of PSt−PMMA copolymer, both polymers are hydrophobic but forms a monolayer at the air−water interface since PMMA is less hydrophobic than PSt.[37,51] The pHeBiB segment of the copolymer used in this study is suspected to be floating on the water subphase instead of being completely immersed in the water even though this part of the macroinitiator is hydrophilic; thus a condensed type monolayer is observed in the $\pi-A$ isotherm.

The discontinuity points in the isotherm signify the different structural organizations that the macroinitiator undergoes upon spreading. Figure 1 shows that at low surface pressures the distances between the macroinitiator molecules are large and interactions are negligible. At surface pressures between 5 and 15 mN/m, the macroinitiator is in a loosely packed conformation. However, as the symmetrical barriers compress the monolayer, the distances between the macroinitiator molecules become smaller but the molecules still have room to move around. At surface pressures between 20 and 30 mN/m, the macroinitiator is in an intermediate conformation. With further compression, the monolayer becomes uniformly and tightly packed. At surface pressure 50 mN/m, the macroinitiator is in a densely packed conformation. At even higher compression, the monolayer is destroyed attaining its collapse point which is seen in Figure 1 at near 71 mN/m (surface tension of water is at 73 mN/m). It is expected that at the lowest surface pressure, there will be a low initiator packing density on the surface. Since the initiating sites are far apart (loosely packed), the polymer chains are expected to be less dense and in a less extended conformation.[20] On the other hand, at higher surface pressures, the polymer chains will attain the most extended conformation due to the closeness in the packing of the initiating sites (densely packed). When the distance between initiating sites is small, the tethered polymer chains attain the brush architecture.[20] However, when the initiator density becomes too large, chain entanglements due to overcrowding of the growing polymer chains can occur.[20,39] As a result, the polymer chains will not fully extend to attain the brush morphology.

The stability of the monolayer was checked by measuring the time dependence of $A$ when $\pi$ was kept constant. At surface pressures 5 and 15 mN/m, stable monolayers are formed. However, at higher surface pressures 20, 30, and 50 mN/m, the occupied areas decreased by about 15−30% until they approached a constant which signified the formation of a stable monolayer. Fukuda et al. reported only a 10% decrease in the occupied area due to the polycondensation reaction between silanol groups formed by the hydrolysis of CTS.[32] In the present study, the macroinitiator is no longer forming a monolayer when compressed to higher surface pressures and instead forming a multilayer which affects its stability over time.

Hysteresis studies were performed by repeatedly measuring the dynamic surface pressure. Figure 2 shows the four repeated compression cycles of the isotherm curves which were performed by compressing the monolayer to the target surface pressure and then expanding it to 0 mN/m (both compression and expansion cycles were done at a constant barrier speed of 10 mm/min). It is clear that a hysteresis is

present since the second isotherm is not superimposable on the first isotherm curve. It has been reported that the rate of expansion is slower than the rate of area increase.[37] Upon expansion, the macroinitiator needs some time to relax back to its initial state. At surface pressures higher than 20 mN/m, it is suspected that a tightly packed monolayer or even multilayer exists on the water surface and the macroinitiator is not reorganizing fast enough during the expansion cycle. However, the hysteresis diminishes after further cycles indicating that a homogeneous monolayer exists on the water surface.

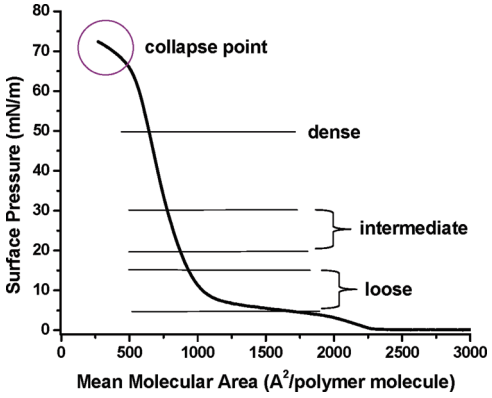


**Figure 1.** Surface pressure ($\pi$) vs mean molecular area ($A$) ($A^2$/polymer molecule) of p(St-*co*-HeBiB) macroinitiator. The different structural organizations the macroinitiator is undergoing are denoted as loose, intermediate, and dense.

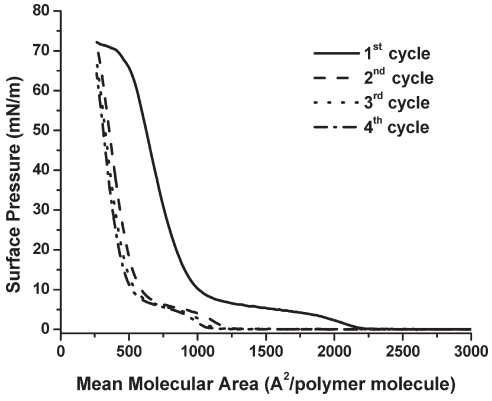


**Figure 2.** Repeated $\pi$-A curves of p(St-*co*-HeBiB): (—) first cycle, (– –) second cycle, (· · ·) third cycle, and (— · —) fourth cycle. Only the compression cycles are plotted.

More in depth hysteresis studies were performed on surface pressures 5, 20, and 50 mN/m. When the expansion is done before the appearance of the plateau in the isotherm curve, virtually no hysteresis exists. Figure 3a shows a compression−expansion cycle at 5 mN/m. It is clear that below 5 mN/m, a reversible isotherm curve is obtained. At higher surface pressures beyond the plateau region, a hysteresis occurs. Figure 3b shows that at 20 mN/m, a slight hysteresis is observed but the monolayer is otherwise homogeneous. (The expansion curve is almost superimposable on the compression curve). However at 50 mN/m, it is clear that the expansion curve does not follow the compression curve. A highly compressed monolayer requires more time to go back to its relaxed conformation during the expansion cycle.[51,52] A high compression puts the macroinitiator in a very dense conformation, and it does not disperse quickly enough after the external pressure is released. Figure 3c shows a minimum in the surface pressure as soon as the expansion begins and then goes back up due to the macroinitiator's structural change.[37a] The compression−expansion cycle at 50 mN/m is therefore an irreversible process.

**Monolayer Deposition.** The macroinitiator monolayer was transferred using the Langmuir−Schaefer (LS) (horizontal immersing) method (Scheme 1b). A clean silicon wafer substrate was treated with hydrofluoric acid to make it a hydrophobic surface. A hydrophobic surface is necessary in order for the pSt segment to be oriented toward the silicon surface leaving the outer surface with the pHeBiB segment (ATRP initiator). Surface monolayers with varying surface pressures were deposited, and the LS macroinitiator films were used for the polymerization of NIPAM (Scheme 1c).

**XPS Analysis.** XPS was used to probe the elemental compositions of the LS films before and after the polymerizations. The atomic concentrations of bromine and silicon in the LS macroinitiator films are of particular interest in this study because they will give insight into the surface coverage of the initiating groups. Quantifying the bromine content in the LS macroinitiator films is especially important because this will dictate the amount of active sites available for the polymerization. Control of the initiator packing density was accomplished by applying various surface pressures during the monolayer deposition. When the macroinitiator monolayer is tightly packed as in the high surface pressures, then the distance between the active sites is very small. In this case, when the brush grows it will be forced to extend away from the surface to avoid the unfavorable steric interactions between adjacent propagating chains.[20] On the other hand, when the surface pressure is low and the macroinitiator is not tightly packed, then the distance between the active sites is large. When there is sufficient space between adjacent macroinitiator molecules, then the growing chains will not

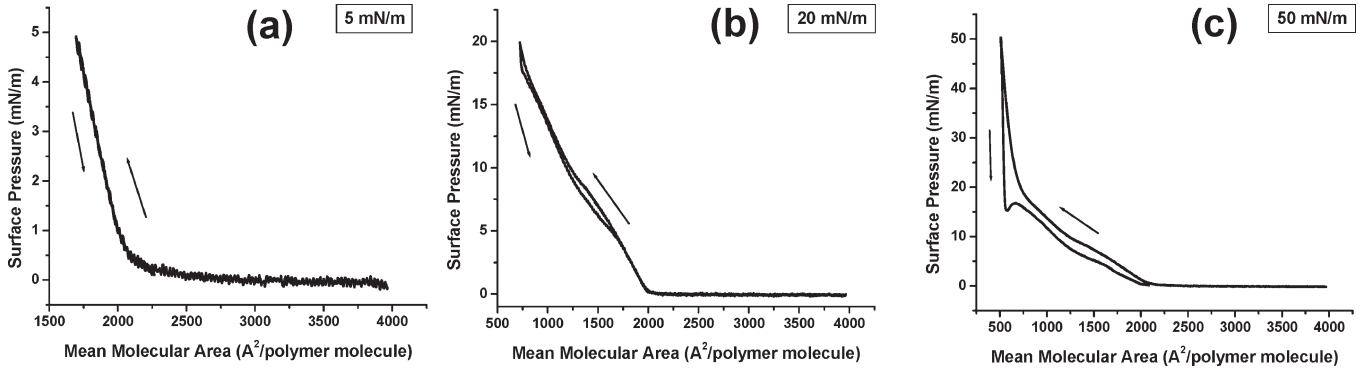


**Figure 3.** Compression−expansion cycles for surface pressures (a) 5, (b) 20, and (c) 50 mN/m. Arrows are drawn as guides for the eyes.

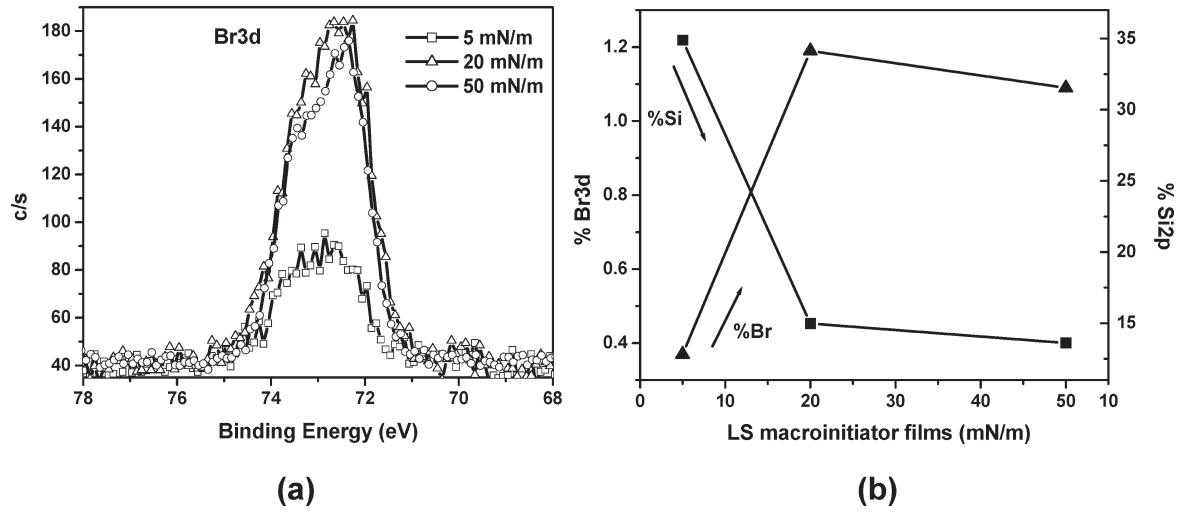


**Figure 4.** (a) High resolution Br 3d XPS spectrum for 5 (□), 20 (△), and 50 (○) mN/m LS macroinitiator films and (b) plot of atomic concentrations of Br 3d (▲) and Si 2p (■) vs surface pressure of the LS macroinitiator films.

be in the most extended conformation and perhaps grow in the mushroom regime.[20]

Figure 4a shows that the Br 3d signal at 73 eV increased from the 5−20 mN/m LS macroinitiator films but decreased going to the 50 mN/m LS macroinitiator film. At low surface pressures, the macroinitiator is in a loosely packed conformation; thus a low bromine concentration of 0.37 was detected for the 5 mN/m LS macroinitiator film. However, as the surface pressure increases, the bromine signal should also increase since at these high surface pressures, the area occupied by the macroinitiator decreases and the monolayer becomes more densely and uniformly packed. Bromine concentrations of 1.19 and 1.09 for the 20 and 50 mN/m LS macroinitiator films were obtained, respectively. On the other hand, the silicon signal (102 eV) decreased accordingly with increasing surface pressure indicating that the surface is almost completely covered for the 50 mN/m LS macroinitiator film. This is due to the fact that more macroinitiator molecules are covering the void spaces on the surface of the substrate resulting from a decrease in the area (Figure 4b). Therefore, the initiator coverage is highest at high surface pressures. Furthermore, AFM images of the LS macroinitiator films show significant differences in the film morphology as a function of surface pressure (Supporting Information Figure S5). The AFM images revealed that the void spaces between the macroinitiator molecules decreased with increasing surface pressure which signified that the surface coverage of the initiating species was increasing with surface pressure.

We conclude that since the $\pi-A$ isotherm curve shows a condensed type monolayer, a monolayer is no longer being formed at surface pressures higher than 20 mN/m and instead a bilayer or even a multilayer is forming on the water surface (Additional AFM images revealing the formation of a multilayer are available in the Supporting Information Figure S5). The Langmuir monolayers of PSt−PMMA diblock copolymer have been shown to form micelles when the monolayer is compressed to high surface pressures with the PSt block occupying the core while the PMMA block occupies the coronae.[37] Similarly, the macroinitiator used in this study behaves in the same way. The pSt segment of the copolymer is driven to aggregate due to its repulsion toward both the water and pHeBiB segment. At even higher compression, the pHeBiB segments are going underneath the pSt core lifting it or extending it up to the air to further avoid its repulsion toward the water.[37] Furthermore, the higher compression starts to bend the backbone of the copolymer. At the air interface, the pSt segment now prefers to be at the coronae while the pHeBiB segment prefers to be at the core. This behavior of pHeBiB will affect its availability to initiate the polymerization.

**Table 1. Ellipsometric Thicknesses and Static Water Contact Angle Measurements for 5, 15, 20, 30, and 50 mN/m LS films Before and After the Polymerization of NIPAM**

| | Thickness (nm) | | Water contact angle (deg) | |
|---|---|---|---|---|
| Surface Pressure (mN/m) | LS | pNIPAM[a] | LS | pNIPAM[a] |
| 5 | 2.5 | 31.8 | 92.4 | 68.6 |
| 15 | 4.9 | 37.6 | 94.0 | 71.6 |
| 20 | 8.6 | 49.0 | 94.0 | 60.9 |
| 30 | 10.6 | 82.5 | 93.0 | 54.2 |
| 50 | 12.2 | 113 | 92.0 | 56.2 |

[a] [NIPAM] = 0.5 M for 1 h polymerization; The brush thicknesses for pNIPAM are listed and not the overall thicknesses.

In addition, the thicknesses of the LS macroinitiator films based on ellipsometric measurements confirmed that thick layers of the macroinitiator were deposited on the surface of the substrates with increasing surface pressures. Table 1 shows that the thicknesses ranged from 2.5 to 12.2 nm for the LS macroinitiator films taken at surface pressures 5, 15, 20, 30, and 50 mN/m. It can be concluded that a monolayer is being deposited for the 5 mN/m LS macroinitiator film. However, at surface pressures higher than 5 mN/m, the macroinitiator is occupying less and less available area on the LB trough. Since it has a relatively small area to occupy, the macroinitiator is bending (twisting) and perhaps stacking on top of each other; thus the monolayer is being destroyed up to its collapse point near 71 mN/m and a bilayer or multilayer is being deposited on the surface. This is more evident when the macroinitiator monolayer is compressed to surface pressures higher than 20 mN/m. The LS macroinitiator films taken at surface pressures 5, 20, and 50 mN/m were then chosen specifically for the ATRP polymerization of NIPAM for in depth analysis of the effect of surface pressure on the initiator packing density.

After the ATRP polymerization of NIPAM, a simple rinsing of the films with a mixture of water and methanol proved to be sufficient to remove residual copper catalyst as evident by the lack of the copper signal in the high resolution XPS scan (Figure 5a inset). However, the XPS showed a

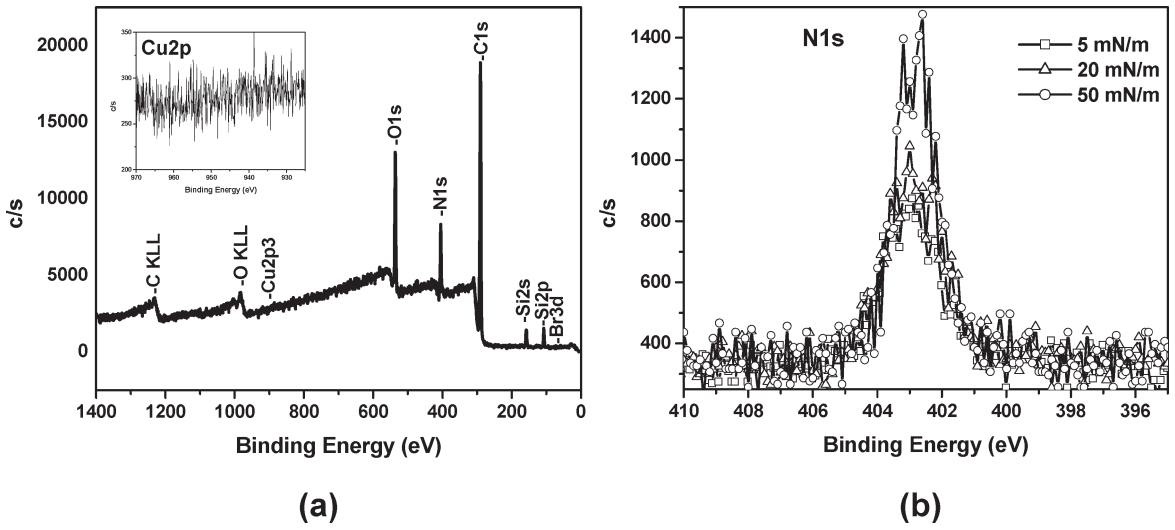


**Figure 5.** (a) XPS survey scan for the LS pNIPAM brush film. The inset shows the Cu 2p spectrum, indicating no incorporation of copper salts in the film after the polymerization. (b) High resolution N 1s XPS spectrum for 5 (□), 20 (△), and 50 (○) mN/m LS brush films.

small bromine signal even though there was no incorporation of the $Cu^{I}Br$ salts. This small bromine signal is due to the livingness of the polymerization.[20,23] The high resolution XPS scan taken from a 113 nm thick 50 mN/m LS brush film revealed an oxygen:nitrogen:carbon (O:N:C) molar ratio of 14.6:9.7:71.6 (expected ratio 12.5:12.5:75.0).[16] Discrepancy between the experimental and actual ratios is due to the thickness of the pNIPAM brush films as well as the adventitious oxygen during the preparation of the films prior to the measurements. Other LS brush films also showed similar O:N:C molar ratios. Even though our initial finding showed that there was a decrease in the bromine signal for the 50 mN/m LS macroinitiator film before the polymerization, this film always gave the thickest pNIPAM brushes. Figure 5b shows the high resolution N 1s signal for the 5, 20, and 50 mN/m LS brush films. The nitrogen signal increased proportionally with surface pressure indicating that the initiator packing density was highest for the 50 mN/m LS brush film.

Since the XPS scans were taken for the LS macroinitiator films in their dry state, we suspect that a macroinitiator surface rearrangement is occurring during the polymerization which was conducted in an aqueous media. To confirm this, we performed static water contact angle measurements. Briefly, the LS macroinitiator films were immersed in a 1:1 by volume of $H_2O$/MeOH for various times and air-dried prior to the contact angle measurements. Figure 6 depicts the structural organization of the macroinitiator at the different stages of the compression. At a low compression where the LB trough area is at its largest, the macroinitiator is depicted to be floating on the water surface in a random coil configuration (or a distorted linear configuration). However, as the compression increases, the monolayer is destroyed and the macroinitiator is no longer being deposited as a monolayer on the substrate surface. Because the macroinitiator is starting to bend and perhaps stack on top of each other as a result of a decrease of the surface area by increasing surface pressure, the pHeBiB segment of the copolymer is being embedded in the underlying layer or hidden within the pSt segment.[37] During the polymerization, however, the polar solvent helps extend the pHeBiB segment so as to be more readily available to initiate the polymerization. After 1 h soaking of the 50 mN/m LS macroinitiator film in the $H_2O$/MeOH solvent, the contact angle only slightly decreased (Table 2). However, there was a gradual decrease in the

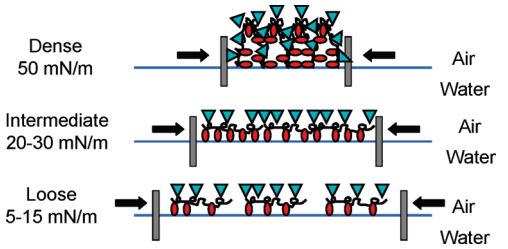


**Figure 6.** Depiction of the structural organization of the macroinitiator at the different stages of compression.

**Table 2. Static Water Contact Angle Measurements for the 50 mN/m LS Macroinitiator Film to Confirm the Surface Rearrangement Occurring During the Polymerization of NIPAM**

| Time (h) | 0 | 1 | 2 | 4 | 8 | 22 |
|---|---|---|---|---|---|---|
| Contact angle (deg) | 92.8 | 92.0 | 91.5 | 89.9 | 86.8 | 81.7 |

contact angle after longer soaking in the mixed solvent. This shows that the embedded or hidden pHeBiB segment of the copolymer slowly comes up to the surface as a result for its affinity toward the polar solvent. The contact angle measurements clearly indicate that the surface is becoming more hydrophilic due to the rich pHeBiB surface. As a consequence, more initiating sites become available for the polymerization resulting in thick pNIPAM brushes. A hydrophilic surface is more evident after soaking the 50 mN/m LS macroinitiator film overnight. Similarly, block copolymers with different preferentiality to a solvent where one segment of the copolymer responds accordingly to a selective solvent while also acting as a nonsolvent for the other block segment have been reported.[53]

**FT-IR Characterization of pNIPAM brushes.** Transmittance-mode FT-IR spectrum was collected from an 82.5 nm thick pNIPAM brush film (LS 30 mN/m, [NIPAM] = 4.4 M, 2 h) (Figure 7). Peak assignments are as follows: the two bands of equal intensity at 1370 and 1390 $cm^{-1}$ are assigned to the deformation of the 2 methyl groups of the isopropyl functionality; 1540 $cm^{-1}$ is the secondary amide −N−H stretching (amide II band) while 1640 $cm^{-1}$ is attributed to the primary amide −C=O stretching (amide I band); 2975 $cm^{-1}$ is due to the $-CH_3$- asymmetric stretching; and 3300 $cm^{-1}$ is due to the secondary amide −N−H stretching. All peak assignments are consistent with previously studied pNIPAM systems.[3,7,16,17]

**PNIPAM Brush Growth.** Neither sacrificial initiator nor deactivator species were added during the ATRP polymerization of NIPAM. Therefore, the polymerization is both surface-confined and surface initiated. We studied the effects of surface pressure on initiator packing density as well as the effects of monomer concentration and polymerization time on the polymer brush growth. Variations in these three parameters led to linear correlations with pNIPAM brush thickness. However, different brush growths were observed for the 5, 20, and 50 mN/m LS brush films. We have confirmed that having a high initiator packing density by virtue of increasing the surface pressure led to very dense pNIPAM brushes. The brush thicknesses ranged from 31.8 to 113 nm for brushes polymerized for 1 h at [NIPAM] = 0.5 M (Table 1). For a comparison, different monomer ratios of styrene to HeBiB (3:3 and 3:6) were synthesized. The LS macroinitiator films for the 3:1, 3:3, and 3:6 macroinitiators were all deposited at 5 mN/m and polymerized using [NIPAM] = 0.5 M for 1 h. It is clearly evident that by increasing the molar ratio of the HeBiB initiating moiety relative to styrene generally leads to thicker pNIPAM brushes. Table 3 shows that the pNIPAM brush thickness using the 3:6 macroinitiator gave a brush thickness higher than the 3:1 macroinitiator deposited at 50 mN/m. Thus, we conclude that varying the applied surface pressure during the monolayer deposition is analogous to varying the molar ratio of the initiating moiety in the copolymer.

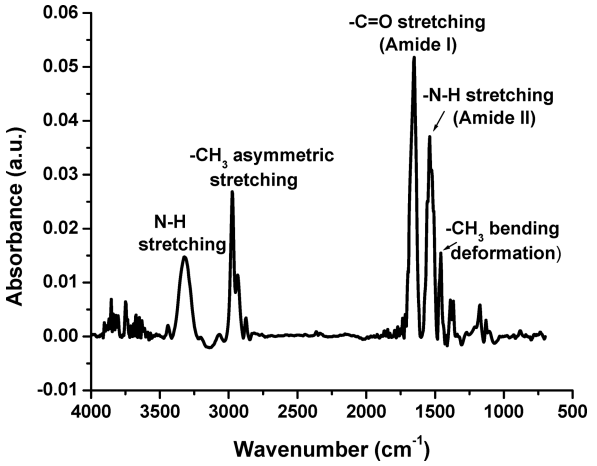


**Figure 7.** FT-IR spectrum of the pNIPAM brushes taken from the 30 mN/m LS brush film. Amides I and II peaks as well as the N−H peak are all indicative of a successful grafting of pNIPAM brushes.

**Table 3. Ellipsometric Thicknesses and Static Water Contact Angle Measurements for the Different Molar Ratios of St:HeBiB**

| | Thickness (nm) | | Water contact angle (deg) | |
|---|---|---|---|---|
| St:HeBiB molar ratio | LS | pNIPAM | LS | pNIPAM |
| 3:1 | 2.5 | 31.8 | 92.4 | 68.6 |
| 3:3 | 2.1 | 55.4 | 83.4 | 68.7 |
| 3:6 | 3.3 | 145.2 | 80.9 | 67.7 |

It can also be concluded that the 50 mN/m LS film gave the thickest pNIPAM brushes regardless of variations in polymerization time and monomer concentration (Figure 8). This signifies that the 50 mN/m LS film had the most available grafting points to which NIPAM can grow as compared to the 5 and 20 mN/m LS films. It can also be seen in Figure 8a that there was a rapid brush growth at 1 h for all three films. However, as the polymerization proceeds longer (>1 h), there was a gradual increase in the brush thickness for all films. A closer examination of Figure 8a reveals that the 20 mN/m LS brush film showed a dramatic increase in thickness after the 2 h polymerization period as compared to 5 and 50 mN/m films. There was approximately a 24 nm increase in brush thickness for the 20 mN/m film going from 2 to 4 h polymerization. This brush growth was almost 4 and 3 times greater than the 5 and 50 mN/m films, respectively. Furthermore, the 20 mN/m pNIPAM brush film nearly doubled in thickness at the 8 h polymerization period. This was a far greater brush growth for the 20 mN/m than for the 5 and 50 mN/m films during the same polymerization period. The different brush growths observed are due to the initiating groups becoming buried underneath the growing propagating chains at longer polymerization times which is more pronounced for the 50 mN/m LS brush film than for 5 and 20 mN/m LS brush films.[5,17,23,26,38] In addition, the kinetics of the macroinitiator surface rearrangement is also a contributing factor in the different brush growths observed.

Huck[38] and Baker[39] both reported thinner brushes with more dilute SAMs consisting of a mixed monolayer. This is

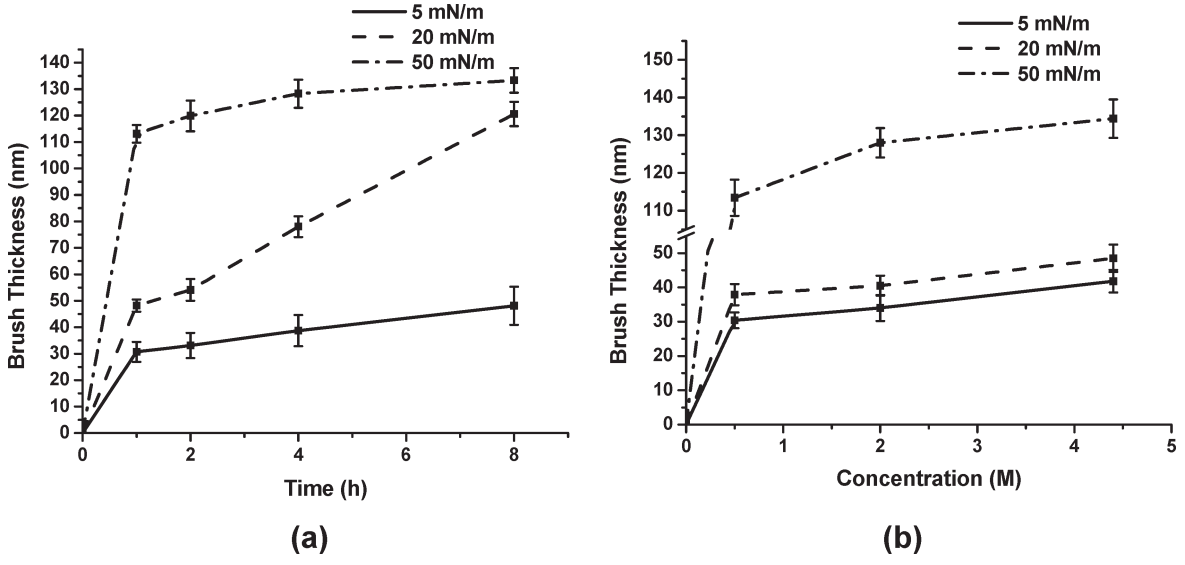


**Figure 8.** Effects of (a) polymerization time (1, 2, 4, and 8 h) and (b) monomer concentration (0.5, 2.0, and 4.4 M) on the polymer brush growth for the (−) 5, (− −) 20, and (− · −) 50 mN/m LS brush films.

consistent with the brush growth for the 5 mN/m LS brush films which can be similarly compared to a dilute SAM since at a low surface pressure, the surface is not concentrated with active sites which the XPS data already confirmed. To explain what is happening with the 20 and 50 mN/m LS brush films, we also considered the dependence of the brush growth on the kinetics of the macroinitiator surface rearrangement. How fast or slow this is occurring on the surface will have a significant impact on the brush growths for the LS brush films. At the lowest surface pressure, there is not much reorganization happening on the surface since the macroinitiator is not tightly packed and not bending nor stacking on top of each other. The contact angle measurement taken from the 5 mN/m LS macroinitiator film after soaking it from 1 to 8 h did not show significant changes. The surface rearrangement is more pronounced at higher surface pressures since the area available for the macroinitiator becomes very small and the monolayer is destroyed where upon the macroinitiator is bending and stacking on top of each other. As discussed earlier, the surface of the 50 mN/m LS macroinitiator film only gradually becomes hydrophilic over time. Although the 50 mN/m LS film is the optimum surface pressure in obtaining the thickest pNIPAM brushes, the 20 mN/m LS brush film showed the greatest increase in brush thickness after the 1 h polymerization period. At 20 mN/m, the macroinitiator has more capacity to rearrange on the surface, and the available area for the macroinitiator to rearrange allows it to get the pHeBiB segment to come out of the surface much faster than for the 50 mN/m LS macroinitiator film. Therefore, the increase in brush growth was largest for the 20 mN/m LS brush films than for 50 mN/m LS brush films. On the other hand, variations in the monomer concentration (2 h polymerization) led to mostly steady increases in the brush thickness regardless of the surface pressure (Figure 8b). It is also interesting to note that there was no clear "cutoff" surface pressure beyond which no further increase in film thickness was observed. Only a slow or stagnant growth was observed with a longer polymerization time.[54]

**Thermal Response of pNIPAM Brushes.** Static water contact angle goniometry was used to investigate the surface wettabilities before and after the polymerization of NIPAM. All of the LS macroinitiator films showed hydrophobic surfaces even though the pHeBiB segment of the copolymer was at the outermost surface. Since a 3:1 ratio of styrene to HeBiB was used to synthesize the copolymer a relatively hydrophobic surface was observed. The contact angle values were all around 90° which is consistent with pSt.[53] In addition, the 3:3 and 3:6 macroinitiators showed less hydrophobic surfaces than the 3:1 macroinitiator reflecting the increase of the pHeBiB segment relative to pSt (Table 3). After the ATRP polymerization of NIPAM, the contact angle values decreased indicating the successful grafting of pNIPAM. The contact angle measurements for the pNIPAM brush films were taken at RT after rinsing the films with room temperature water and air-dried. No trend in the contact angle values was observed for the pNIPAM films. Contact angle values between 60 and 70° were obtained for the films regardless of the variations in surface pressure, polymerization time, and monomer concentration.[55]

The thermal responsive nature of pNIPAM brushes was investigated in two ways. First, we used static water contact angle to measure the changes in the surface wettability above and below the LCST (32 °C) (Figure 9). Second, we performed an *in situ* AFM imaging using a temperature controller to probe the changes in the film morphology as a function of temperature in the dry state (Figure 10). At RT,

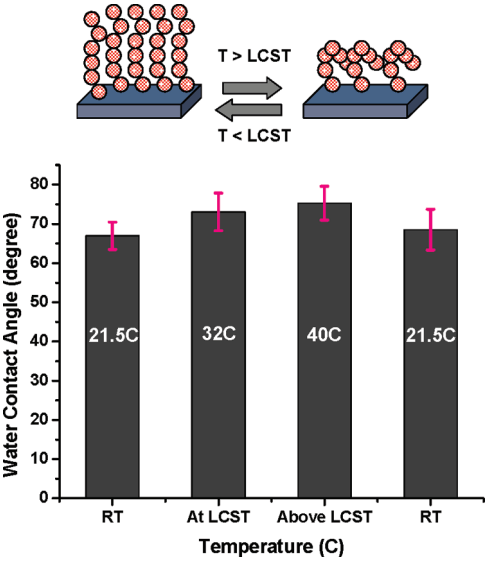


**Figure 9.** Static water contact angle measurement for the pNIPAM brushes as a function of temperature. The surface changed from hydrophilic to hydrophobic below and above the LCST (32 °C). The contact angle values were averaged on three different spots on the film.

the pNIPAM chains are in an extended conformation due to the hydrogen bonding with water and the amide group.[10−12] After soaking the film at RT water for 20 min and air-dried, a value of 66.97° was obtained indicating a hydrophilic surface. Increasing the temperature to 32 °C showed an increase in the water contact angle value (73.06°). Above the LCST, the pNIPAM chains adopt a collapse conformation due to the breaking of the hydrogen bonds with the amide group.[10−12] A value of 75.27° was obtained at 40 °C which was indicative of a hydrophobic surface. The initial contact angle value was not reached as the film was allowed to go back to room temperature which indicated that the pNIPAM chains have not reached equilibrium.

Although the pNIPAM brush film responded accordingly with temperature, the small changes in the contact angle values are attributed to several factors. First, grafted pNIPAM brushes exhibit a broader LCST (from ∼10 to 40 °C) than pNIPAM in bulk aqueous solution (LCST 32 °C).[9] In the present study, the temperature range between 21 and 40 °C might not have been enough to observe noticeable changes between the hydrophobic and hydrophilic states of pNIPAM brushes. Second, the brush film was soaked in water at the specified temperature for only 20 min and perhaps a longer soaking period, i.e., 1 h, might provide a larger temperature response. Furthermore, it has been reported that the temperature dependent behavior of grafted pNIPAM is greatly affected by the molecular weight of the polymer chains as well as the grafting density.[10,11] High molecular weight or high density pNIPAM brushes tend to show a large conformational change as a function of temperature. In the current study, the 5 mN/m pNIPAM film which was polymerized with [NIPAM] = 0.5 M at 1 h was used for the temperature dependent experiments. This particular film had a thickness close to 32 nm which is perhaps not dense enough to observe a fast and quantitative conformational change as compared to previously studied pNIPAM systems.[3,5,7,9−12]

Figure 10 shows a $3.5 \times 3.5$ $\mu$m AFM (phase image) film morphology as a function of temperature. At RT, pNIPAM is in its hydrated form and swell as a result of the hydrogen bonding. As the temperature was increased to 32 °C, a smoother film was obtained. However, as the temperature

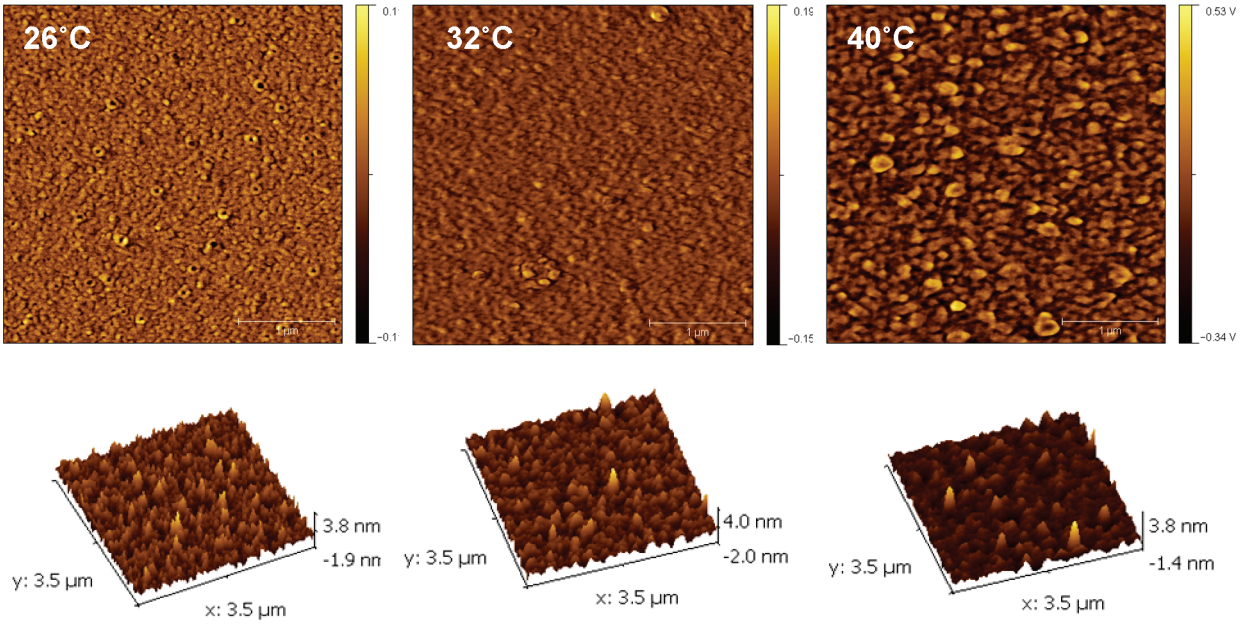


**Figure 10.** *In situ* AFM phase and corresponding 3D images (3.5 × 3.5 $\mu$m) of the pNIPAM brushes for the 5 mN/m LS brush film ([NIPAM] = 0.5 M, 1 h) above and below the LCST (32 °C). Globular domains become more apparent upon heating to 40 °C due to the phase separation of the brushes.

was increased to 40 °C, it was clear that more globular domains appeared. The aggregation behavior of the pNIPAM brushes is due to the breaking of the hydrogen bonds with the amide group of pNIPAM.[10−12] As the pNIPAM expels water above the LCST, phase separation occurs as the water molecules must reorient themselves around the isopropyl functionality. Although only slight changes in contact angle values were observed above and below the LCST, the AFM images confirmed that the surface morphology does indeed respond to temperature.

## Conclusions

The surface immobilization of an amphiphilic macroinitiator carrying an ATRP initiator was demonstrated by using the LS technique, and the temperature responsive films were fabricated by the ATRP polymerization of NIPAM. The surface grafting density increased with increasing surface pressures indicating that the initiator packing density was at its highest when the macroinitiator monolayer was deposited at surface pressure 50 mN/m compared to surface pressures 5 and 20 mN/m. Consequently, thicker brushes and a higher nitrogen signal were obtained for the 50 mN/m LS brush films. On the basis of the static water contact angle measurements, a macroinitiator surface rearrangement was occurring during the polymerization which was conducted in an aqueous media. As a consequence of the mixed solvent used, the hydrophilic part of the copolymer carrying the ATRP initiator rearranged so that it became more available on the surface to initiate the polymerization and thus impacted the brush growths for the 5, 20, and 50 mN/m LS brush films. By varying the temperature above and below the LCST (32 °C) of pNIPAM, different surface wettabilities and morphologies were observed. Applications toward other smart surfaces can be used with the current LS-SI-ATRP system.

**Acknowledgment.** The authors would like to acknowledge funding from NSF DMR-06-02896, DMR-1006776, CBET-0854979, and the Robert A. Welch Foundation, E-1551. We would also like to thank KSV Instruments (Biolin), Agilent Technologies, Malvern Instruments, and Optrel for their technical support.

**Supporting Information Available:** Text discussing experimental details and figures showing $^1$H NMR, TGA, DSC, and FT-IR of p(St-*co*-HeBiB) macroinitiator, stability of the LS monolayer, AFM images of the LS macroinitiator films, and $\pi-A$ isotherm of the macroinitiator with different monomer ratios. This material is available free of charge via the Internet at http://pubs.acs.org.

## References and Notes

(1) Liu, Y.; Zhao, M.; Bergbreiter, D. E.; Crooks, R. M. *J. Am. Chem. Soc.* **1997**, *119*, 8720–8721.
(2) Park, M.; Deng, S.; Advincula, R. C. *J. Am. Chem. Soc.* **2004**, *126*, 13723–13731.
(3) Fulghum, T. M.; Estillore, N. C.; Vo, C.-D.; Armes, S. P.; Advincula, R. C. *Macromolecules* **2008**, *41*, 429–435.
(4) Park, Y. S.; Ito, Y.; Imanishi, Y. *Langmuir* **1998**, *14*, 910–914.
(5) Ista, L. K.; Mendez, S.; Perez-Luma, V. H.; Lopez, G. P. *Langmuir* **2001**, *17*, 2552–2555.
(6) Mayo, E. I.; Lochner, E. J.; Stiegman, A. E. *J. Phys. Chem. B* **1999**, *103*, 9383–9386.
(7) Pan, Y. V.; Wesley, R. A.; Luginbuhl, R.; Denton, D. D.; Ratner, B. D. *Biomacromolecules* **2001**, *2*, 32–36.
(8) Piech, M.; Bell, N. S. *Macromolecules* **2006**, *39*, 915–922.
(9) Balamurugan, S.; Mendez, S.; Balamurugan, S. S.; O'Brien, M. J.; Lopez, G. P. *Langmuir* **2003**, *19*, 2545–2549.
(10) Yim, H.; Kent, M. S.; Mendez, S.; Balamurugan, S. S.; Balamurugan, S.; Lopez, G. P. *Macromolecules* **2004**, *37*, 1994–1997.
(11) Plunkett, K. N.; Zhu, X.; Moore, J. S.; Leckband, D. E. *Langmuir* **2006**, *22*, 4259–4266.
(12) Annaka, M.; Yahiro, C.; Nagase, K.; Kikuchi, A.; Okano, T. *Polymer* **2007**, *48*, 5713–5720.
(13) Zhu, X.; DeGraaf, J.; Winnik, F. M.; Leckband, D. *Langmuir* **2006**, *20*, 10648–10656.
(14) Wang, W.; Zhang, C.; Wang, S.; Zhao, J. *Macromolecules* **2007**, *40*, 9564–9569.
(15) Jones, D. M.; Smith, J. R.; Huck, W. T. S.; Alexander, C. *Adv. Mater.* **2002**, *14*, 1130–1134.
(16) Tu, H.; Heitzman, C. E.; Braun, P. V. *Langmuir* **2004**, *20*, 8313–8320.
(17) Kaholek, M.; Lee, W-K.; Ahn, S-J.; Ma, H.; Caster, K. C.; LaMattina, B.; Zauscher, S. *Chem. Mater.* **2004**, *16*, 3688–3696.
(18) (a) Takei, Y. G.; Matsukata, M.; Aoki, T.; Sanui, K.; Ogata, N.; Kikuchi, A.; Sakurai, Y.; Okano, T. *Bioconjugate Chem.* **1994**, *5*, 577–582. (b) Kanazawa, H.; Yamamoto, K.; Matsushima, Y.; Takai, N.; Kikuchi, A.; Sakurai, Y.; Okano, T. *Anal. Chem.* **1996**, *68*, 100–105. (c) Kobayashi, J.; Kikuchi, A.; Sakai, K.; Okano, T. *Anal. Chem.* **2001**, *73*, 2027–2033.
(19) Belder, G. F.; Brinke, G. T.; Hadziioannou, G. *Langmuir* **1997**, *13*, 4102–4105.

(20) *Polymer Brushes: Synthesis, Characterization, Application*; Advincula, R. C.; Brittain, W. J.; Caster, K. C.; Ruhe, J.; Eds.; Wiley-VCH: Weinheim, Germany, 2004.
(21) (a) Prucker, O.; Ruhe, J. *Langmuir* **1998**, *14*, 6893–6898. (b) Prucker, O.; Ruhe, J. *Macromolecules* **1998**, *31*, 602–613. (c) Biesalski, M.; Ruhe, J. *Macromolecules* **2003**, *36*, 1222–1227.
(22) Matyjaszewski, K.; Xia, J. *Chem. Rev.* **2001**, *101*, 2921–2990.
(23) Matyjaszewski, K.; Miller, P. J.; Shukla, N.; Immaraporn, B.; Gelman, A.; Luokala, B. B.; Siclovan, T. M.; Kickelbick, G.; Vallant, T.; Hoffmann, H.; Pakula, T. *Macromolecules* **1999**, *32*, 8716–8724.
(24) Moad, G.; Rizzardo, E.; Thang, S. H. *Aust. J. Chem.* **2006**, *59*, 669–692.
(25) Hawker, C. J.; Basman, A. W.; Harth, E. *Chem. Rev.* **2001**, *101*, 3661–3688.
(26) Ramakrishnan, A.; Dhamodharan, R.; Ruhe, J. *Macromol. Rapid Commun.* **2002**, *23*, 612–616.
(27) (a) Wu, T.; Efimenko, K.; Genzer, J. *J. Am. Chem. Soc.* **2002**, *124*, 9394–9395. (b) Wu, T.; Efimenko, K.; Vlcek, P.; Subr, V.; Genzer, J. *Macromolecules* **2003**, *36*, 2448–2453. (c) Wu, T.; Gong, P.; Szleifer, I.; Vlcek, P.; Subr, V.; Genzer, J. *Macromolecules* **2007**, *40*, 8756–8764.
(28) (a) Chen, X. Y.; Armes, S. P.; Greaves, S. J.; Watts, J. F. *Langmuir* **2001**, *20*, 587–595. (b) Vo, C-D.; Schmid, A.; Armes, S. P. *Langmuir* **2007**, *23*, 408–413. (c) Edmondson, S.; Vo, C-D.; Armes, S. P. *Macromolecules* **2007**, *40*, 5271–5278.
(29) Edmondson, S.; Vo, C.-D.; Armes, S. P.; Unali, G-F.; Weir, M. P. *Langmuir* **2008**, *24*, 7208–7215.
(30) Fulghum, T. M.; Patton, D. L.; Advincula, R. C. *Langmuir* **2006**, *22*, 8397–8402.
(31) Jain, P.; Dai, J.; Grajales, S.; Saha, S.; Baker, G. L.; Bruening, M. L. *Langmuir* **2007**, *23*, 11360–11365.
(32) Ejaz, M.; Yamamoto, S.; Ohno, K.; Tsujii, Y.; Fukuda, T. *Macromolecules* **1998**, *31*, 5934–5936.
(33) Ejaz, M.; Ohno, K.; Tsujii, Y.; Fukuda, T. *Macromolecules* **2000**, *33*, 2870–2874.
(34) Yamamoto, S.; Ejaz, M.; Tsujii, Y.; Matsumoto, M.; Fukuda, T. *Macromolecules* **2000**, *33*, 5602–5607.
(35) Ejaz, M.; Yamamoto, S.; Tsujii, Y.; Fukuda, T. *Macromolecules* **2002**, *35*, 1412–1418.
(36) Ulman, A. *An Introduction to Ultra-Thin Films: From Langmuir-Blodgett to Self-Assembly*: Academic Press: Boston, MA, 1991.
(37) (a) Seo, Y.; Im, J-H.; Lee, J-S.; Kim, J.-H. *Macromolecules* **2001**, *34*, 4842–4851. (b) Seo, Y.; Paeng, K.; Park, S. *Macromolecules* **2001**, *34*, 8735–8744.
(38) Jones, D. M.; Brown, A. A.; Huck, W. T. S. *Langmuir* **2002**, *18*, 1265–1269.
(39) Bao, Z.; Bruening, M. L.; Baker, G. L. *Macromolecules* **2006**, *39*, 5251–5258.
(40) (a) Ionov, L.; Zdyrko, B.; Sidorenko, A.; Minko, S.; Klep, V.; Luzinov, I.; Stamm, M. *Macromol. Rapid Commun.* **2004**, *25*, 360–365. (b) Liu, Y.; Klep, V.; Zdyrko, B.; Luzinov, I. *Langmuir* **2005**, *21*, 11806–11813.
(41) Yamamoto, S.; Ejaz, M.; Tsujii, Y.; Fukuda, T. *Macromolecules* **2000**, *33*, 5608–5612.
(42) Tsujii, Y.; Ejaz, M.; Yamamoto, S.; Fukuda, T.; Shigeto, K.; Mibu, K.; Shinjo, T. *Polymer* **2002**, *43*, 3837–3841.
(43) Fu, G. D.; Kang, E. T.; Neoh, K. G.; Lin, C. C.; Liaw, D. J. *Macromolecules* **2005**, *38*, 7593–7600.
(44) Crosby, R.; Haw, J. F. *Macromolecules* **1987**, *20*, 2326–2328.
(45) Brinkhuls, R. H. G.; Schouten, A. J. *Macromolecules* **1991**, *24*, 1487–1495.
(46) (a) Kumaki, J. *Macromolecules* **1986**, *19*, 2258–2263. (b) Kumaki, J. *Macromolecules* **1988**, *21*, 749–765.
(47) Parker, J.; Shereshefsky, J. L. *J. Phys. Chem.* **1954**, *58*, 850–853.
(48) Kumaki, J.; Nishikawa, Y.; Hashimoto, T. *J. Am. Chem. Soc.* **1996**, *118*, 3321–3322.
(49) Kawaguchi, M.; Sauer, B. B.; Yu, H. *Macromolecules* **1989**, *22*, 1735–1743.
(50) Capan, I.; Capan, R.; Tanriserver, T.; Can, S. *Mater. Lett.* **2005**, *59*, 2468–2471.
(51) Goncalves da Silva, A. M.; Filipe, E. J. M.; d'Oliveira, J. M. R.; Martinho, J. M. G. *Langmuir* **1996**, *12*, 6547–6553.
(52) Eisenberg, J. Z.; Lennox, R. B. *Macromolecules* **1992**, *25*, 6547–6555.
(53) Granville, A. M.; Boyes, S. G.; Akgun, B.; Foster, M. D.; Brittain, W. J. *Macromolecules* **2004**, *37*, 2790–2796.
(54) Liu, Y.; Klep, V.; Zdyrko, B.; Luzinov, I. *Langmuir* **2004**, *20*, 6710–6718.
(55) Takei, Y. G.; Aoki, T.; Sanui, K.; Ogata, N.; Sakurai, Y.; Okano, T. *Macromolecules* **1994**, *27*, 6163–6166.